Low-frequency cortical activity is a neuromodulatory target that tracks recovery after stroke

Dhakshin S. Ramanathan[1,2,3,4,5,11], Ling Guo[1,6,11], Tanuj Gulati [1,7,11], Gray Davidson[1,2,3], April K. Hishinuma[1,7], Seok-Joon Won[1,7], Robert T. Knight[8,9], Edward F. Chang[10], Raymond A. Swanson[1,7] and Karunesh Ganguly [1,7]*

Recent work has highlighted the importance of transient low-frequency oscillatory (LFO; <4 Hz) activity in the healthy primary motor cortex during skilled upper-limb tasks. These brief bouts of oscillatory activity may establish the timing or sequencing of motor actions. Here, we show that LFOs track motor recovery post-stroke and can be a physiological target for neuromodulation. In rodents, we found that reach-related LFOs, as measured in both the local field potential and the related spiking activity, were diminished after stroke and that spontaneous recovery was closely correlated with their restoration in the perilesional cortex. Sensorimotor LFOs were also diminished in a human subject with chronic disability after stroke in contrast to two non-stroke subjects who demonstrated robust LFOs. Therapeutic delivery of electrical stimulation time-locked to the expected onset of LFOs was found to significantly improve skilled reaching in stroke animals. Together, our results suggest that restoration or modulation of cortical oscillatory dynamics is important for the recovery of upper-limb function and that they may serve as a novel target for clinical neuromodulation.

An emerging view of the primary motor cortex (M1) sees it as an engine for movement governed by transient oscillatory dynamics that are present during both the preparation and the generation of movement[1–7]. Movement-related, low-frequency quasi-oscillatory (LFO) activity, at the level of both spiking and local field potentials (LFPs), has also been observed in the intact non-human primate M1 and human motor regions during reaching tasks[2–5,8–13]. Such quasi-oscillatory activity can be as brief as 1–2 cycles for rapid movements or longer during sustained movements, and seems to be closely correlated with sub-movement timing[4,5,14]. They may also be related to the multiphasic muscle activations that are required for precise kinetics during actions[15,16]. Thus, LFOs seem to represent an intrinsic property of motor circuits that are involved in the production of fast and accurate movements.

Here, we hypothesized that monitoring and manipulating movement-related LFOs after stroke may offer new avenues to understand motor recovery. Previous research using invasive electrophysiological approaches has largely focused on measurements of nervous system function that occur at rest and/or away from motor tasks[17–20]. For this reason, surprisingly, little is known about how stroke and recovery affects task-related neural dynamics at the level of single neurons and mesoscopic circuit function. Non-invasive studies in human subjects have found that electroencephalogram (EEG) movement-related potentials (for example, slow cortical potentials[21–23]) are affected by stroke[24–27]. Furthermore, changes in the slow cortical potential are correlated with motor impairments post-stroke[26]. However, one limitation of EEG is the uncertainty regarding specific anatomical generators and neural processes that contribute to the recorded potentials; moreover, slow cortical potentials include various pre-movement and movement-related phemonenon[22,23], further limiting their interpretation.

A generative model of cortical dynamics in both the healthy and the recovering nervous system may guide the development of novel, closed-loop neuromodulatory approaches that dynamically target transient task-related processes. Despite our knowledge that neural networks are highly non-stationary, the vast majority of previous studies applying electrical or magnetic stimulation to the brain post-injury have applied it continuously, without explicitly targeting intrinsic neural dynamics[28–30] and with a primary goal of generally increasing excitability and/or plasticity[31–33]. However, recent work has suggested that therapeutic electrical stimulation can be used to target phasic oscillatory dynamics[34,35], an idea that has been successfully implemented in Parkinson's disease[36] and epilepsy[37]. Implementing such an approach post-stroke requires detailed knowledge of normal and abnormal neural dynamics and a better understanding of how to modulate them. Here, we aimed to identify neurophysiological dynamics associated with skilled execution; assess whether these same dynamics are related to recovery; and finally, to evaluate whether temporally precise electrical neuromodulation of these dynamics can improve motor function post-stroke.

[1]Neurology Service, San Francisco Veterans Affairs Medical Center, San Francisco, CA, USA. [2]Mental Health Service, San Francisco Veterans Affairs Medical Center, San Francisco, CA, USA. [3]Department of Psychiatry, University of California, San Francisco, San Francisco, CA, USA. [4]Mental Health Service, VA San Diego Health System, San Diego, San Diego, CA, USA. [5]Department of Psychiatry, University of California, San Diego, San Diego, CA, USA. [6]Neuroscience Graduate Program, University of California, San Francisco, San Francisco, CA, USA. [7]Department of Neurology, University of California, San Francisco, San Francisco, CA, USA. [8]Helen Wills Neuroscience Institute, University of California, Berkeley, Berkeley, CA, USA. [9]Department of Psychology, University of California, Berkeley, Berkeley, CA, USA. [10]Department of Neurosurgery, University of California, San Francisco, San Francisco, CA, USA. [11]These authors contributed equally: Dhakshin S. Ramanathan, Ling Guo, Tanuj Gulati. *e-mail: karunesh.ganguly@ucsf.edu

Results

The motor cortex exhibits LFO activity during execution of a skilled forelimb reaching task. Long Evans male rats ($n = 4$) were implanted with microwire arrays in M1 after learning a skilled forelimb reach task[38] (Fig. 1a,b). Animals were trained over multiple days using an automated reach-box[39]. In addition to movement-related spiking activity in M1 in well-trained rats[40,41] (Fig. 1c), we also observed LFO activity at the level of both the LFP and spiking activity (Fig. 1d, example trial, Supplementary Fig. 1 for a description of quasi-oscillatory population dynamics and Supplementary Fig. 2a for additional trial examples). We found strong movement-related power predominately in lower LFP frequencies that began prior to reach onset; neurons showed coherent spiking with the LFP at these frequencies (Fig. 1e,f). We quantified these effects by calculating the mean 1.5–4-Hz LFP power and spike-field coherence (SFC; from −0.25 to 0.75 s around the reach onset) across channels/units from all animals. There was a significant increase in both power (mixed-effects model with 118 channels and 4 rats as random effect: $t(117) = 6.77$, $P = 5.37 \times 10^{-10}$) and SFC (mixed-effects model with 170 units and 4 rats as random effect: $t(170) = 8.07$, $P = 1.24 \times 10^{-13}$) during the reach as compared to the pre-reach 'baseline'. Because power and SFC were computed for each trial and then averaged, these values are not related to the mean evoked 'event-related potential' (ERP), but rather to single-trial dynamics. Together, these findings indicate that the rodent M1 also demonstrates similar task-related LFO activity described in non-human primates[2–4,14]. A dynamic increase in SFC associated with movement suggests one of two possibilities: single units and LFPs could both be phase locked to the motor action and therefore simply seem phase locked to each other; or, by contrast, there may be independent phase locking between units and LFPs. One approach of teasing this apart is to subtract out the average ERP, which represents the dominant 'phase-locked' LFP activity across trials, and then recalculate power or SFC. By subtracting the ERP, we were left with 'induced' oscillations (the non-phase-locked changes in power associated with movement); thus, the subsequent SFC measure indicates a more direct relationship between LFP phase and spiking that is less contaminated by phase-locked LFP activity to the reach. Using this approach, we again found a strong increase in task-evoked low-frequency SFC (Supplementary Fig. 2b) and power (Supplementary Fig. 2c) evoked by reaching.

One advantage of LFP recordings over spiking is the stability over long periods of time[14,42,43]. By contrast, spike recordings are easily affected by micro-motion, making it difficult to follow the same ensemble across days. Notably, we found remarkable stability in the measured task-related low-frequency LFP power across trials and days (Supplementary Fig. 2d–f). Finally, LFP measurements provide information about mesoscale organization of neural activity[8,44] (Fig. 1g). Interestingly, we found that only a subset of channels demonstrated an increase in task-related low-frequency power; there appeared to be spatial clustering of channels, suggesting that M1 activation is not uniform at the mesoscale level.

The middle cerebral artery occlusion stroke model diminishes LFO activity. After collecting electrophysiological data in the healthy state (Fig. 1), we performed a distal middle cerebral artery (MCA) occlusion stroke on these same animals (Fig. 2a). Induction of this type of stroke could be performed without perturbing implanted electrodes, thus allowing for a direct comparison of neural activity pre-stroke and post-stroke in the same animals and cortical region. Stroke in the distal MCA model resulted in a large area of damage within the sensorimotor cortex (Fig. 2b and Supplementary Fig. 3a). Animals were tested again after at least a 5-day rest post-stroke; neural activity was measured again once animals could attempt reaches and at least occasionally retrieve the pellet (Supplementary Fig. 3b shows example hand trajectories).

The stroke resulted in impaired skilled motor function (Fig. 2c). Importantly, neural probes were positioned such that at least some electrodes remained in viable tissue (Fig. 2b and Supplementary Fig. 3a); even post-stroke, single units remained on a subset of electrodes (Fig. 2d). There were fewer units post-stroke (an average of 1.45 versus 0.453 units per channel pre-stroke versus post-stroke), but those that remained continued to demonstrate task-related increases in activity, although demonstrating significantly less modulation on average (Fig. 2d and Supp Fig. 3c,d). Reach-related LFOs were perturbed (Fig. 2e–i). Low-frequency SFC was reduced after stroke (Fig. 2g, mixed-effects model: $t(221) = 7.45$, $P = 2.07 \times 10^{-12}$; Supplementary Fig. 3e,f); changes in firing rate could not explain the observed changes in SFC (Supplementary Fig. 3g,h). To further probe the relationship between spiking activity and LFP using a method that is not confounded by potential changes in firing rate, we calculated the preferred phase of spiking. We found strong phase locking to the trough of the low-frequency LFP pre-stroke and no preferred phase of spiking post-stroke (Supplementary Fig. 3i,j). LFP power also reduced after stroke (Fig. 2h,i, mixed-effects model: $t(100) = 6.01$, $P = 3.06 \times 10^{-8}$; Supplementary Fig. 3k,l). As task-related units were present, the loss of the reach-related LFP power was not simply a product of probes being in infarcted tissue (Fig. 2i). The decrease in LFP power was also not due to changes in movement speed; power was not correlated with movement duration (Supplementary Fig. 3m). As before, subtracting the mean ERP to isolate 'induced' activity did not significantly change the results (Supplementary Fig. 3n–q). Together, these analyses clearly demonstrated that stroke resulted in a striking loss of LFOs and phase-locked quasi-oscillatory spiking activity.

Functional recovery correlates with the restoration of LFO activity. Having observed a clear decrease in LFOs in M1 after stroke, we next wondered whether the recovery of function might be associated with its restoration in the perilesional cortex. Because of variability in the location of damage after the distal MCA occlusion[45], we performed this next set of experiments using a focal photothrombotic stroke model[46] to generate a relatively reproducible area of damage (Supplementary Fig. 4a); thus, this allowed us to know a priori the location of the perilesional cortex and to target neural probes to the appropriate rostral location where rehabilitation-induced plasticity has been shown to occur[17,47]. Immediately after stroke induction, a 16- or 32-channel microelectrode array was implanted anterior to the site of the injury[48] (Fig. 3a,b). Animals were given 5 days to recover from the stroke and electrode implantation; they then underwent motor training on the same task to assess the relationship between recovery and task-related LFOs in the perilesional cortex. Injury resulted in impaired motor performance ($73.6 \pm 12.21\%$ versus $35.1 \pm 11.9\%$; two-tailed, paired t-test: $t(5) = 3.35$, $P = 0.0204$), which improved over the course of subsequent training ($69.1 \pm 9.01\%$ last session; two-tailed, paired t-test comparing the first versus the last session: $t(5) = 3.03$, $P = 0.0290$; Fig. 3c and see Supplementary Fig. 4b for example paw trajectories).

With recovery of function, spiking activity in the perilesional cortex became sharper, more task related and more similar to that observed in the healthy M1 (Fig. 3d and Supplementary Fig. 4c,d). There was a clear emergence of low-frequency task-related activity in both spiking and LFP in the perilesional cortex (Fig. 3e–k). This increase in LFO can be observed in single-trial examples (Fig. 3e) and across trials/sessions within the same animals (Fig. 3f). Statistically, there was a strong increase in the 1.5–4-Hz SFC (Fig. 3g,h, mixed-effects model: $t(387) = 8.94$, $P = 1.59 \times 10^{-17}$; Supplementary Fig. 4e). Changes in the SFC could not be explained by changes in firing rate (Supplementary Fig. 4f–i). In addition, 1.5–4-Hz power increased significantly (Fig. 3i,j, mixed-effects model: $t(175) = 3.11$, $P = 0.00217$; Supplementary Fig. 4j,k). Moreover, subtracting the ERP did not change the results (Supplementary Fig. 4l–o).
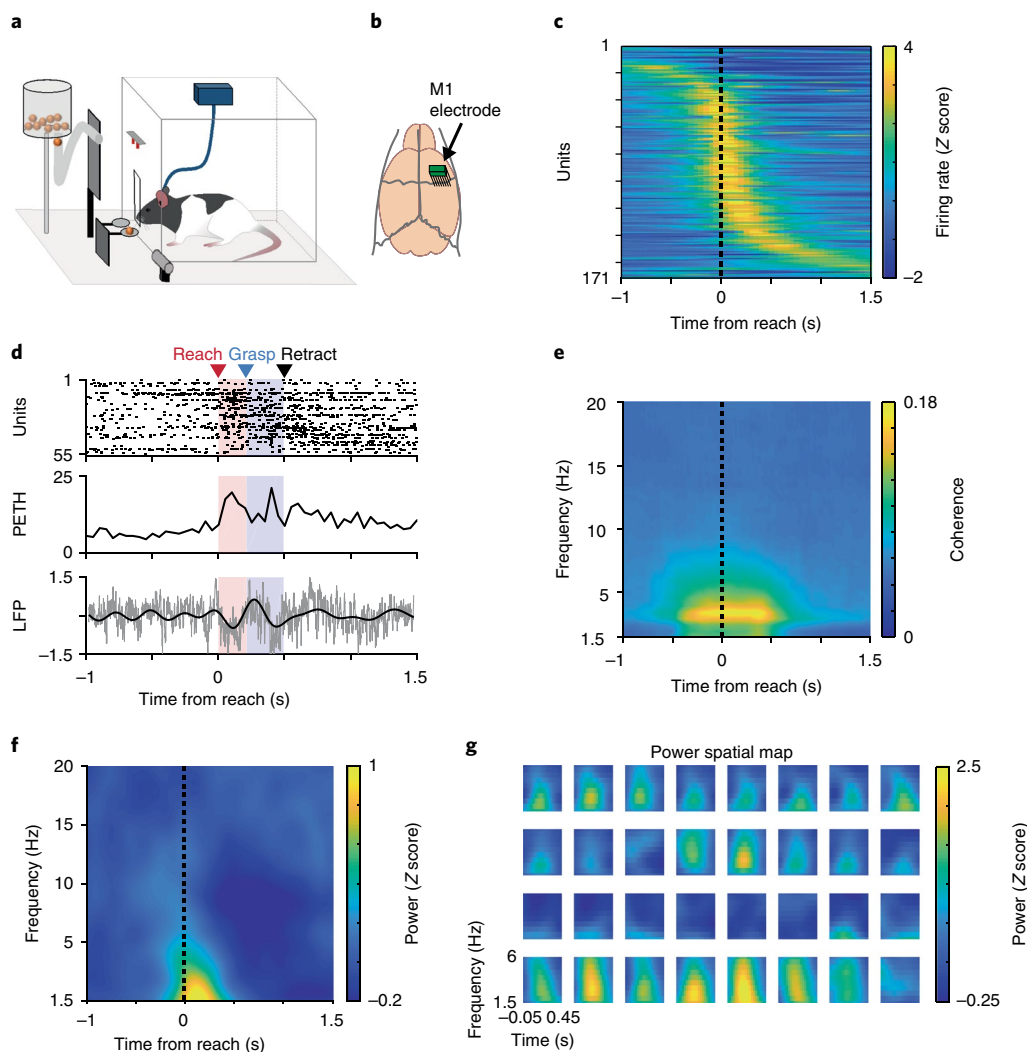
Fig. 1 | LFO activity during a skilled forelimb reaching task in healthy rats. a, The behavioral setup for the skilled forelimb reaching task with simultaneous neurophysiological recording. **b**, Fixed 32-channel microwire arrays were implanted in the motor cortex. **c**, Z-scored unit firing rate changes (171 units from 4 rats) aligned to the reach onset (black dotted line, same labeling conventions apply to **e** and **f**). **d**, A single trial example of brief LFO activity during reaching (top: spike raster of all the units in this example trial; middle: a population peri-event time histogram (PETH) for all spikes shown on the top panel; bottom: Z-scored raw LFP in gray and the LFP filtered from 1.5–4 Hz (black line) from an example channel). This trial is a representative example of trials that show high SFC and high power, as quantified subsequently. **e**, The mean SFC across 171 units from 4 rats. **f**, The mean LFP power across 118 channels from 4 rats. **g**, A 4×8 grid of electrodes from one animal, in actual spatial configuration, with 375-μm spacing in the y direction and 250-μm spacing in the x direction, plotting only power from 1.5 to 6 Hz and from −0.05 to 0.45 s from reach onset.

There was a significant positive relationship between the restoration of low-frequency power and improvements in accuracy on the task (Fig. 3f, example animal, and Fig. 3l, all animals, Pearson's correlation $r = 0.576$, $P = 1.18 \times 10^{-7}$). There was also a significant correlation between the restoration of the SFC and recovery of function ($r = 0.554$, $P = 4.60 \times 10^{-7}$) and between single-unit modulation change and recovery ($r = 0.561$, $P = 3.01 \times 10^{-7}$). A multivariate linear regression model with all three variables significantly predicted motor improvements ($r = 0.737$, $P = 1.28 \times 10^{-11}$). Each variable had significant partial correlation ($r = 0.428$, $P = 2.21 \times 10^{-4}$ for power; $r = 0.339$, $P = 0.00410$ for the SFC; $r = 0.398$, $P = 6.29 \times 10^{-4}$ for unit modulation), suggesting that all variables could independently account for the variance in recovery of function.

Movement-related LFOs are impaired in human stroke. We next assessed whether our observed phenomena in rodent models were relevant in human stroke[46] by re-analyzing invasive human electrocorticography (ECoG) data collected from three human subjects undergoing invasive epilepsy monitoring to identify seizure foci[8,44]. Physiological data were recorded during a center-out reach task in which subjects were instructed to wait for a start cue and then reach as fast as possible to a target (Fig. 4a). Two of these patients had intact sensorimotor cortices (hereafter nonstroke or NS1/NS2); however, the third patient had experienced an ischemic cortical stroke 4 years prior to the monitoring (hereafter stroke subject) (Fig. 4b). The stroke subject had persistent motor deficits involving arm and hand movements (Fugl–Meyer upper-limb score of 35). He also showed impairments in the speed of execution. The reaction time from 'Go' to movement onset (that is, the rise in the mean electromyography, EMG) was slower for the affected versus the unaffected arm (reaction time of 635 ± 40 and 423 ± 72 ms, respectively, $t(56) = -2.7$, $P = 0.009$, two-tailed, two-sample t-test). Similarly, the reach time from movement onset to target acquisition was longer for the affected arm (reach time of $1{,}266 \pm 58$ ms versus 914 ± 51 ms, $t(56) = -4.42$, $P = 4.65 \times 10^{-5}$, two-tailed, two-sample t-test).
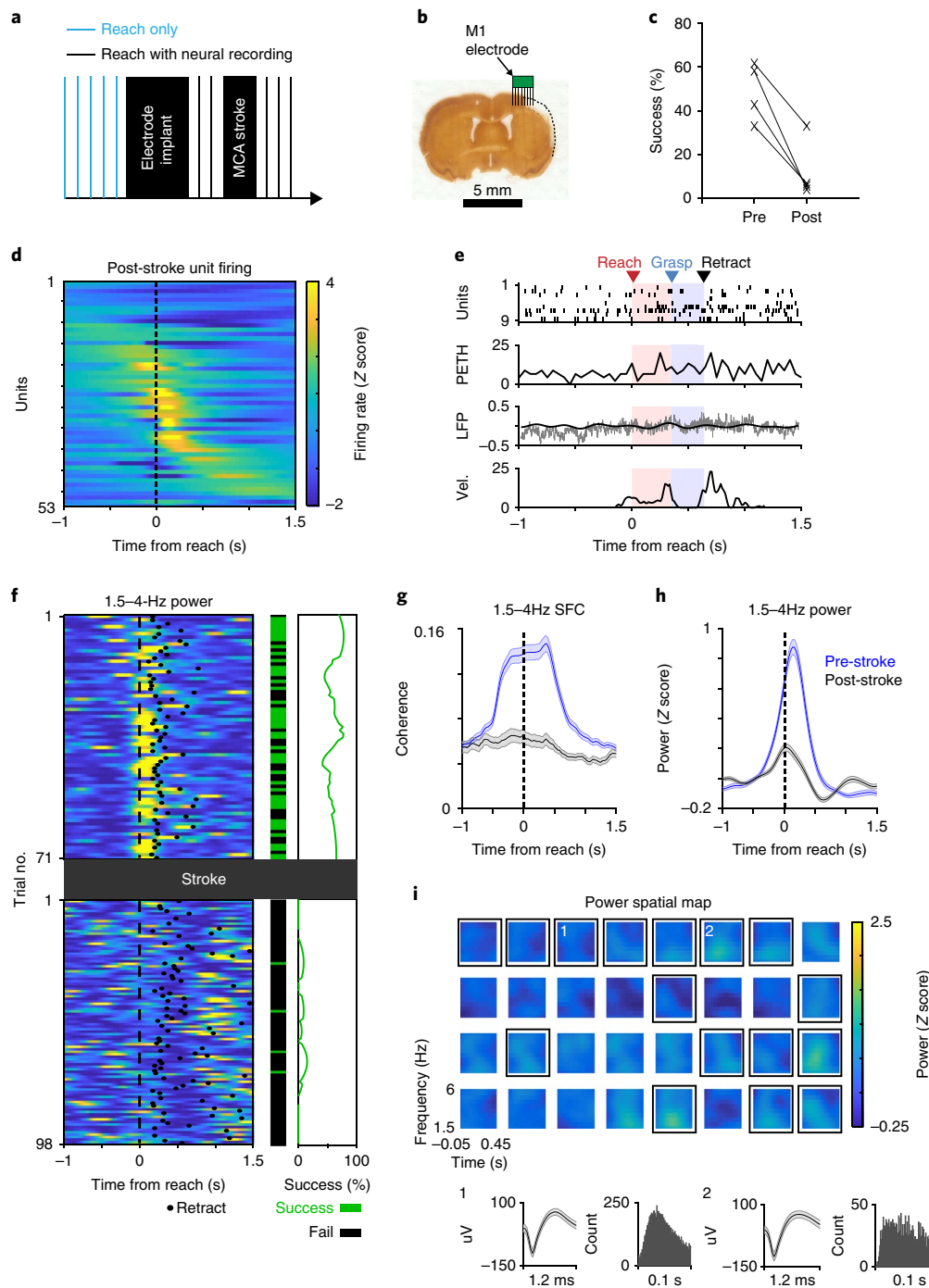
Fig. 2 | Stroke diminished LFO activity in M1. a, Experimental paradigm. After the MCA stroke, we continued recording neural activity from M1 during the reach task in the same animals as in Fig. 1. **b**, A histological section showing the stroke and the approximate location of electrodes from one animal. We performed a similar histological analysis in all four animals to verify that there was some observable lesion resulting from the stroke. **c**, The pellet retrieval success rate before (mean: 48.9%, s.d.: 13.4%) and after (mean: 12.4%, s.d.: 13.8%) the distal MCA stroke in 4 rats (two-sided, paired *t*-test: $t(3) = 5.77$, $P = 0.010$). **d**, *Z*-scored unit firing rate changes relative to the reach onset (53 units from 4 rats). **e**, Single trial example of diminished LFO activity. The labeling convention is the same as in Fig. 1d. The bottom panel shows paw velocity (Vel.) in arbitrary units. This is representative of trials that show low SFC and LFP power, quantified in subsequent panels (**g,h**). **f**, The trial-by-trial low-frequency LFP power decrease after stroke shown in an example channel, paralleled by a decrease in the success rate. Left panel: 1.5–4-Hz LFP power; middle panel: the trial-by-trial success rate; right panel: the success rate smoothed over 25 trials. Only trials in which rats reached and touched the pellet were included. This is representative of a channel that shows high power prior to the stroke and low power after, as quantified in subsequent panels (**g,h**). **g**, Quantification of 1.5-4-Hz SFC before ($n = 171$ units) and after ($n = 53$ units) stroke in 4 rats. The solid lines show the mean and the shaded areas are the s.e.m. Black dotted line indicates reach onset time. **h**, Quantification of changes in the low-frequency (1.5–4 Hz) LFP power after stroke, comparing all paired channels ($n = 101$) from all 4 animals. The solid lines show the mean and the shaded areas are the s.e.m. Black dotted line is reach onset. **i**, An example grid of channels from the same rat as in Fig. 1 and in the same scale. Channels with spiking activity are enclosed by black borders. Insets 1 and 2 show the mean unit waveforms (black line; the shaded area is the s.e.m.) and the inter-spike interval histograms from two selected channels. All four animals demonstrated a similar loss of low-frequency power across channels after the stroke.
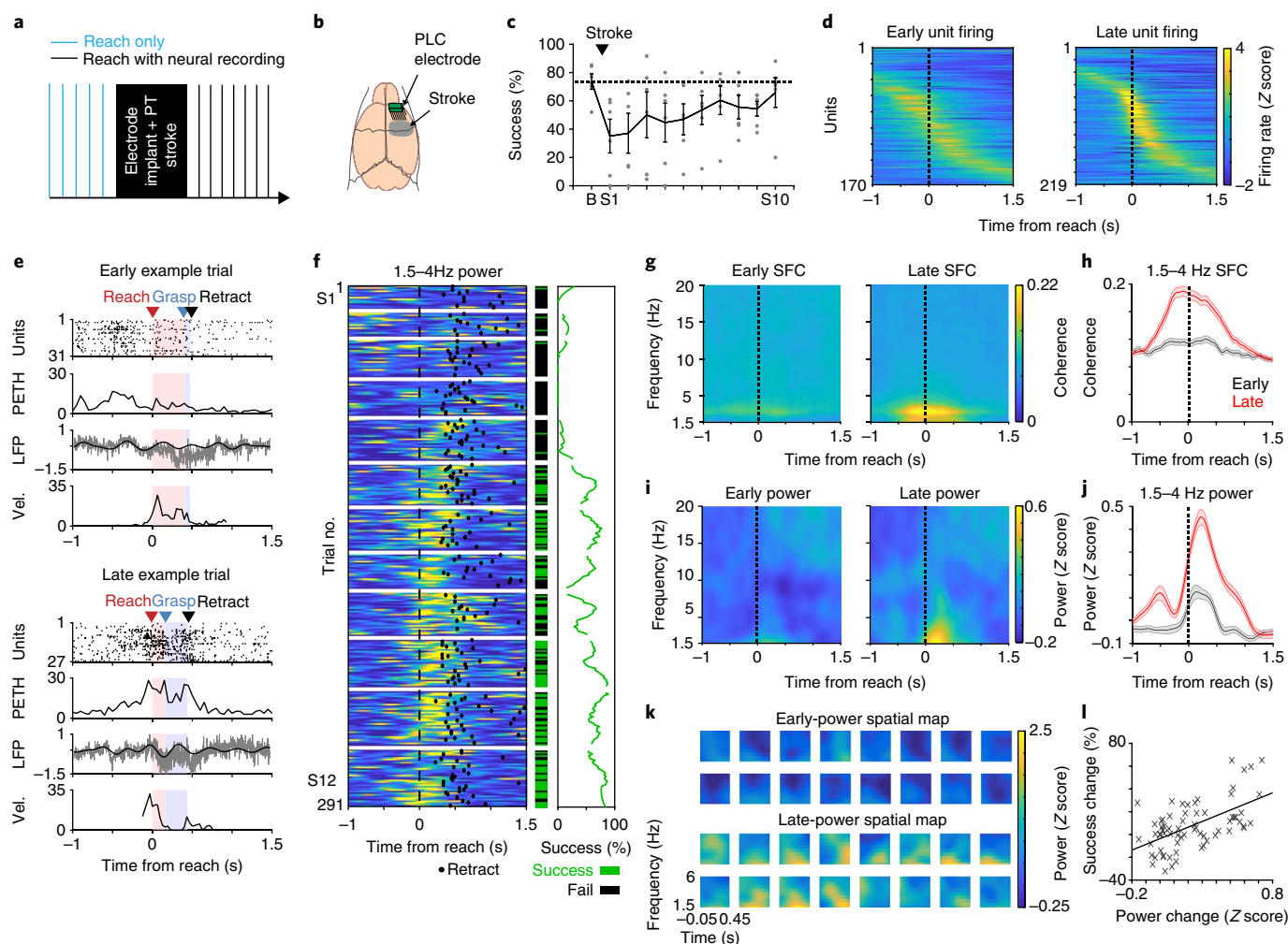
Fig. 3 | Restoration of LFOs in the perilesional motor cortex tracked motor recovery. a, Experimental paradigm. PT = photothrombotic. **b**, Schematic showing the location of the stroke and the electrode. PLC, perilesional cortex. **c**, The mean pellet retrieval success rate before the stroke and during rehabilitation training sessions ($n = 6$; error bars show the s.e.m. and the gray dots show the mean of the individual rats). Session 1 (S1) was 1 week post-stroke for all. Each animal typically attempted 2 sessions of 25–35 trials each per day. B, baseline. **d**, Firing rate changes relative to the reach onset in early (the first) and late (the last) sessions (for all units from all six rats). **e**, An example of increased LFO activity with rehabilitation, both at the level of spiking and at the level of the LFP, in two trials with similar paw velocity. The labeling convention is the same as in Fig. 1d. **f**, An example channel from one animal showing a trial-by-trial 1.5–4-Hz LFP power increase, along with success rate increase, over the course of rehabilitation training. Quantification of this effect across channels is in panels **i** and **j**. The labeling convention is the same as in Fig. 2f. The horizontal white lines separate the training sessions. **g,h**, The mean SFC, calculated from units ($n = 170$ early, $n = 219$ late) in all 6 animals. Black dotted line indicates reach onset. The shaded areas in **h** are the s.e.m. and the solid lines represent the mean. **i,j**, The mean LFP power across channels ($n = 176$) from all 6 animals in early and late trials. Black dotted line indicates reach onset. The shaded areas in **j** are the s.e.m. and the solid lines are the mean. **k**, Spatial topography of the low-frequency LFP power increase. The plot shows example channels from one animal. All six animals showed similar patterns of recovery, as quantified in panels **i** and **j**. **l**, A scatter plot showing significant correlation between the restoration of low-frequency power (mean: 1.5–4-Hz power from –0.25 to 0.75 s around the reach onset) and improvements on the motor task ($r = 0.576$, two-tailed Pearson's correlation; $P = 1.18 \times 10^{-7}$). Each x represents one session from one rat ($n = 72$ sessions), with values normalized for each animal to the first session post-stroke.

For ECoG recordings from NS1/NS2, we found evidence for robust task-related LFOs centered around the sensorimotor cortex (Fig. 4c). The time course and pattern of this activity (Fig. 4d) appeared to closely resemble that observed in rodents (Fig. 1f). However, in the stroke subject, there was a striking loss of this sensorimotor reach-related low-frequency activity (Fig. 4c–e). The mean normalized 1.5–4-Hz LFP power for sensorimotor electrodes (from −300 ms to 300 ms) was significantly positive for NS1/NS2: NS1, normalized mean activity: 0.55 ± 0.2 ($n = 18$ sensorimotor electrodes, two-tailed, one-sample t-test: $t(17) = 7.16$, $P = 2 \times 10^{-6}$) and 0.93 ± 0.25 in NS2 ($n = 16$ SM electrodes, two-tailed, one-sample t-test: $t(15) = 5.47$, $P = 6.5 \times 10^{-5}$), whereas the stroke subject showed no significant increase in power (-0.12 ± 0.12, $n = 91$ SM

electrodes, two-tailed, one-sample t-test: $t(90) = -1.03$, $P = 0.304$). There was a highly significant difference in task-related low-frequency power between the stroke subject and NS1/NS2. We analyzed all channels from all subjects comparing healthy versus stroke, including subject as a factor in the model to account for differences between the two healthy subjects. Using this approach, we found a highly significant overall effect ($F(2,122) = 9.80$, $P = 1.13 \times 10^{-4}$) and, more importantly, a highly significant effect of stroke ($F(1,122) = 18.76$, $P = 3.1 \times 10^{-5}$). It is possible that these results were observed because the LFO was dominant near the central sulcus in healthy subjects, whereas in stroke, due to cortical reorganization, the LFO could be observed in other regions of the brain. Indeed, previous analyses of the data from the stroke subject demonstrated
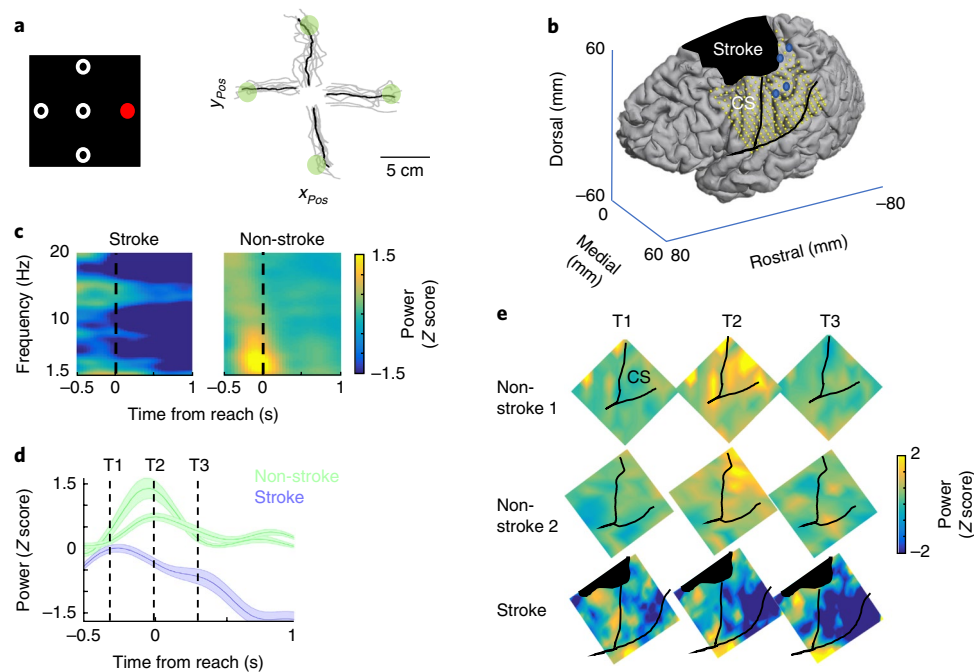
Fig. 4 | Movement-related LFOs in the sensorimotor cortex of a human stroke patient relative to non-stroke subjects. a, Left: the center-out paradigm used in patients with ECoG recordings. In each trial, subjects were given a hold cue, followed by a 'reach' cue (red) that indicated which target to move to. Right: an example of trajectories in the stroke patient. Movement-related data were recorded from two subjects with no stroke and one stroke subject. Analyses were collapsed across all movement directions in each subject. **b**, The placement of the ECoG grid in the stroke subject and the location of the stroke. Blue dots indicate where intracortical stimulation evoked hand movements. CS = central sulcus. **c**, Event-related spectral power across sensorimotor electrodes from one intact subject and the stroke subject. The power is normalized to a baseline time period for each channel (activity prior to the hold cue). This experiment was not repeated on a subsequent day. **d**, The temporal plot of the mean low-frequency power (1.5–4 Hz; solid lines) from sensorimotor electrodes in each of the 2 intact subjects (NS1: n = 18 electrodes; NS2: n = 16 electrodes; and the stroke subject: n = 91 electrodes). The shaded areas show the s.e.m. for each subject across electrodes. T1, time point 1. **e**, A spatiotemporal plot at the three time points indicated in panel **d**, demonstrating an increase in the low-frequency power along the CS (sensorimotor strip) in the two healthy subjects and the absence of this power in the stroke subject. The Z-score scale displayed to the right of the image is identical for all subjects and time points. Experiments were not repeated in these subjects.

intact high-gamma activity away from the central sulcus that was correlated with muscle synergies, suggesting functional reorganization[44]. Thus, to account for functional reorganization, we selected channels that showed increased activity in the high-gamma band between −300 and 300 ms prior to reach. This was performed blind to the location, in an unbiased manner for all three subjects. Using this method of functional[49] rather than anatomical selection, we found overall similar results (Supplementary Fig. 5). These results suggest that LFO activity is a common electrophysiological signature of healthy motor circuit function across both rats and humans.

Direct current stimulation modulates LFO activity in the rodent cortex. A key goal of this project was to assess whether we could modulate task-related oscillations and thereby develop a targeted neuromodulation approach post-stroke. Previous research has demonstrated that direct current stimulation (DCS) can modulate spiking activity[50] and ongoing, carbachol-induced gamma-oscillatory dynamics[34]. It has also been recently reported that LFO activity observed during ketamine anesthesia is similar to the brief, low-frequency spiking–LFP dynamics during natural reaching[3]. To study the effects of DCS in vivo, we analyzed the effects of DCS on M1 LFO activity during ketamine anesthesia (10 rats, 11 sessions). Neural recordings during anesthesia are of substantially greater quality; we can move electrodes to optimize location near neurons and greatly increase signal to noise, which is a requirement for monitoring spiking during stimulation. After anesthesia induction, we implanted epidural electrodes for stimulation and M1 microwire electrodes to measure neural activity (Fig. 5a). Baseline spiking/LFP

activity was recorded for 15 minutes, followed by recordings during the application of a 1–5-minute long DCS (mean duration: 2.909 ± 0.607 minutes, mean amplitude: 106.364 ± 44.526 µA) via the epidural electrodes adjacent to the implanted recording electrodes. We found that DCS could effectively modulate ongoing LFO dynamics during ketamine anesthesia (Fig. 5b–d). Specifically, DCS significantly increased LFP power in the lower frequencies (Fig. 5b, 1.5–4-Hz LFP power, baseline: 0.266 ± 0.047 and with DCS: 0.314 ± 0.062; two-tailed, paired t-test: t(10) = − 2.49, P = 0.032). DCS also generally increased phasic spiking (Fig. 5c) and significantly increased 1.5–4-Hz SFC (Fig. 5d, SFC without DCS: 0.278 ± 0.016 and during DCS: 0.316 ± 0.022; one-tailed, paired t-test: t(49) = −1.73, P = 0.0452). Moreover, 40% of neurons changed their firing rate significantly. More specifically, 30% of neurons increased and 10% decreased their firing rates over the baseline period. SFC analyses were performed after controlling for any firing rate changes[51]. This was important as the firing rate changed significantly for these neurons at a population level (n = 50, two-tailed, paired t-test: t(49) = −2.65, P = 0.0109).

Task-dependent DCS facilitates improved recovery of motor function post-stroke. We next performed experiments to assess whether shorter pulses of DCS (< 5 seconds in duration), applied directly during reaching behaviors, could improve motor function after stroke. Importantly, we avoided the significantly longer-duration stimulation (for example, continuous stimulation for 5 minutes) that is known to induce long-lasting changes in excitability[31,32], as we wanted to specifically assess whether transient

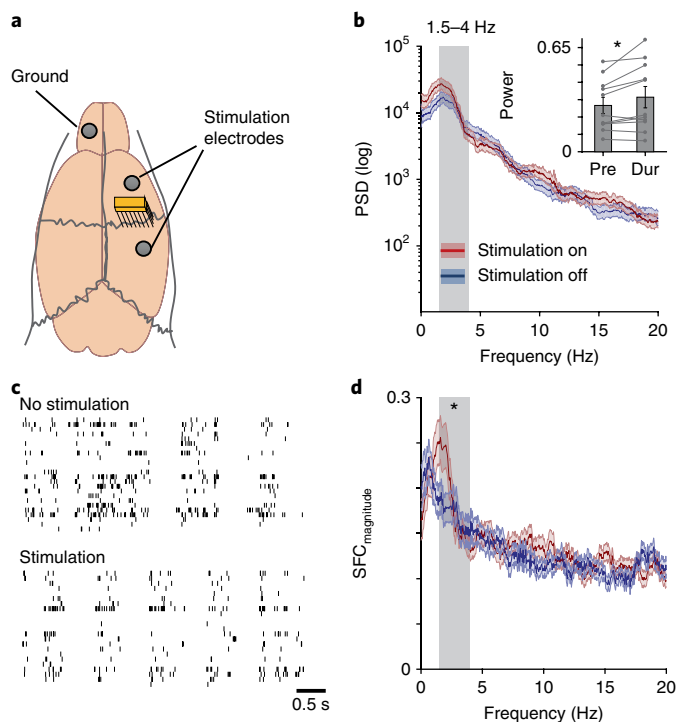**Fig. 5 | LFO activity increased with DCS in acute (anesthetized) recording sessions. a**, Recording and stimulation arrangement in acute experiments. **b**, LFP power before and during DCS shown in one session. PSD = power spectral density. The gray shaded area shows the 1.5–4-Hz frequency range. The solid lines in blue and red show the mean and the shaded areas show the s.e.m. The inset shows the 1.5–4-Hz power in pre-DCS (Pre) and during DCS (Dur) in all 11 sessions from 10 rats (the mean and the s.e.m. are shown in bar plots with individual values; two-tailed, paired t-test: $t(10) = -2.493$, $*P = 0.032$). **c**, Spiking activity of the same neurons from a session before and during stimulation, showing increased coherent spiking during DCS. **d**, The mean SFC (the dark red and blue solid lines— conventions as previous) of 50 neurons from 10 rats. The blue and red shaded areas represent the s.e.m. The 1.5–4-Hz SFC (the gray shaded area) increased with DCS (one-tailed, paired t-test: $t(49) = -1.727$, $*P = 0.045$).

'on-demand' stimulation could induce behavioral improvements. For these experiments, animals underwent either a photothrombotic ($n = 4$) or distal MCA ($n = 3$) stroke induction and were implanted with cranial screws for stimulation both anterior and posterior to the injury site (Fig. 6a). Animals then underwent motor training until their level of performance plateaued (see Methods); DCS was then performed. Stimulation experiments occurred 20–150 days after the stroke, with no clear relationship between the time after stroke and the efficacy of stimulation. We compared the effects of stimulation with a 'no stimulation' and a 'sham stimulation' condition (Fig. 6b). Using this paradigm, we found that stimulation effects were 'on-demand' and did not persist across blocks, allowing us to test, daily, all three conditions (blocks of trials of no stimulation, sham stimulation or stimulation). The order of these blocks was pseudo-randomized across days in every animal and across sessions. We calculated the percentage improvement in accuracy for each daily stimulation and sham condition relative to the no stimulation condition for that day, and then calculated the mean improvement across days for each animal to perform statistics. Animals showed an improvement of $73 \pm 12\%$ in accuracy following stimulation compared with no stimulation (one-sample, two-tailed t-test: $t(6) = 6$, $P = 9.6 \times 10^{-4}$) and a non-significant change of $-4 \pm 5\%$ in the

sham stimulation group (one-sample, two-sided t-test: $t(6) = -0.77$, $P = 0.47$; Fig. 6c). There was also a significant difference in the observed behavioral effects between the stimulation and the sham conditions (two-tailed, paired t-test: $t(6) = 4.91$, $P = 0.003$). Further analyses describing stroke-type and variation in effects across days as well as additional experiments using cathodal stimulation are described in the Methods.

We next assessed whether DCS could enhance task-related LFOs. We recorded neural signals from 4 post-stroke rats with persistent deficits while they attempted the reach-to-grasp task over a total of 24 sessions (a total of 1,031 trials, 532 reach trials with 'stimulation on' and 499 trials without DCS). Simultaneous recording of neural signals during brief epochs of stimulation is particularly challenging as the stimulation onset/offset triggers large distortions in both the LFP and spiking. Thus, we had to substantially alter the stimulation parameters. We used significantly lower current amplitudes ($81.654 \pm 12.414 \mu A$ versus $321.4 \pm 12.2 \mu A$ in the behavioral experiments above), longer-duration pulses (DCS pulses were typically 15-seconds long) and more distant stimulation sites to accommodate the recording probe (see Methods). The average Z-scored 1.5–4-Hz LFP power was higher during DCS trials (0.201 ± 0.076) than during no stimulation trials (0.059 ± 0.038, $t(1,029) = 7.425$, $P = 2.361 \times 10^{-13}$, mixed-effects model; Fig. 6d–f). We observed a trend towards increased accuracy with DCS in this set of animals: $21.069 \pm 14.963\%$ increase (one-tailed, paired t-test: $t(3) = -1.830$, $P = 0.082$). The reduced efficacy was probably the result of the lower current amplitude used. Consistent with this notion are the data from our early pilot experiments (see Methods) and in the behavior-only animals (Fig. 6c) where stimulation currents of $>150 \mu A$ per screw were required to observe consistent behavioral improvements.

Finally, we designed a separate set of stimulation experiments using 1-second long pulses in a new group of animals to replicate the previous effect and more precisely determine the temporal relationship between electrical stimulation and the neural processes underlying reach control after stroke. More specifically, we pseudo-randomly varied the timing of stimulation onset (in blocks of 25 trials) relative to the trial onset (that is, the door opened to allow reach) (Fig. 6g). Importantly, the only parameter that varied was the timing of the stimulation onset relative to this cue; stimulation was delivered on all trials. Next, we calculated the time between stimulation onset and the actual reach onset (ΔT) for each trial, thereby allowing us to precisely assess the relationship between the timing of stimulation and the change in motor function. We then calculated the percentage accuracy for all trials at a particular ΔT by binning all trials in a window of ± 50 ms around that time point (100-ms bins). We observed a significant improvement in accuracy only when ΔT occurred between 500 and 400 ms from the reach (Fig. 6h; two-tailed, one-sample t-test: $t(3) = 9.035$, $P = 0.0458$, Bonferroni– Holm correction for 16 time points; also see Supplementary Fig. 6 for individual animal traces). It is important to note that, with 1-second pulses, stimulation around this time point probably maximally overlaps with the expected LFO (visualized on the plot, although the mean LFP trace was taken from different animals). Given the brief duration of stimulation pulses, 1-second long stimulation pulses at other times probably began or ended during the LFO; and, interestingly, did not seem to be beneficial. Together, our data demonstrate that DCS improved motor function in a temporally restricted manner and could enhance the LFO after stroke, suggesting a novel mechanism by which neuromodulation can work to improve motor function post-stroke.

Discussion
Our results identified LFO activity as an important neurophysiological marker of skilled motor control. We found evidence of such activity at the level of neural spiking and the LFP during the
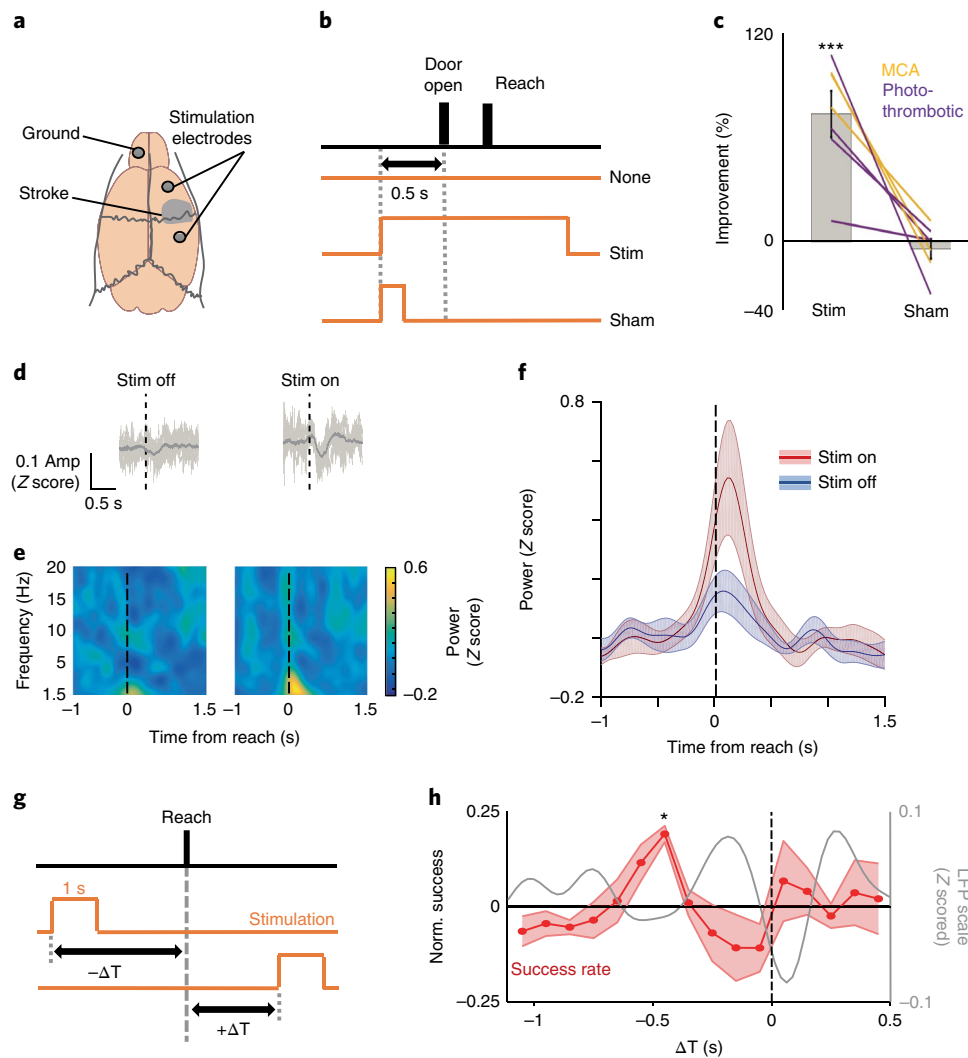
Fig. 6 | Task-dependent DCS improved motor function post-stroke. a, The placement of cranial screws for stimulation in relation to the stroke lesion along with the ground screw. **b,** Pseudo-randomized stimulation (Stim) design indicating the trial with either DCS, a 'sham stimulation' control (Sham; stimulation turned on for only 200 ms) or no stimulation. **c,** The effects of DCS versus sham stimulation on motor accuracy on the skilled forelimb reach task post-stroke. The bar plots demonstrate the mean and the s.e.m. percentage improvement in accuracy, and the solid lines show the effects in each animal ($n = 7$). We performed one-sample, two-sided t-test separately for the stimulation ($t(6) = 6.004$, ***$P = 9.6 \times 10^{-4}$) and the Sham ($t(6) = -0.77$, $P = 0.47$) groups, followed by a paired, two-sample, two-sided t-test to compare the effects between groups ($t(6) = 4.91$, $P = 0.003$). **d,** The mean raw LFP trace (solid dark gray lines; $n = 70$ trials stimulation off, $n = 66$ trials stimulation on) from one animal comparing DCS on versus off; the light gray lines show 6 example single-trial traces. The black dashed lines indicate the reach onset time. Quantification is performed in panel **e. e,f,** The mean LFP power (mean 1.5–4-Hz power for **f**) for all sessions ($n = 13$ stimulation on sessions, $n = 11$ stimulation off sessions) across 4 animals. The solid blue and red lines in panel **f** are the mean and the shaded areas are the s.e.m. The black dashed line indicates the reach onset time. **g,** A pseudo-randomized stimulation onset design depicting how a 1-s stimulation was triggered in relation to the reach onset. ΔT was negative if the stimulation occurred prior to reach onset, and it was positive if stimulation onset occurred after reach onset. **h,** The percentage accuracy as a function of ΔT ($n = 4$ animals). The shaded area displays the s.e.m. (* indicates significant improvement in accuracy at ΔT between 500 ms and 400 ms from the reach onset; $t(3) = 9.035$, *$P = 0.046$, after Bonferroni–Holm correction for 16 different time points). The gray line shows the mean 1.5–4-Hz LFP from healthy animals, taken from Fig. 1.

performance of a dexterous task in rats and in ECoG signals in human subjects without stroke. In both rodents and humans, cortical stroke seemed to significantly disrupt low-frequency activity and its reemergence strongly tracked recovery of motor performance in rats. We also found that pulses of electrical stimulation enhanced entrainment of spiking, increased LFO activity and also improved motor performance in animals with persistent deficits. Consistent with this model, electrical stimulation was primarily effective when it started prior to and lasted through the reach, suggesting that applied electrical fields directly modulated neural dynamics linked to task execution.

There is growing literature demonstrating that LFO activity can capture reach dynamics[21,22,26]; our results provide evidence that this activity is also relevant during recovery. Are these events truly 'oscillatory', given their relatively brief nature? In this study, we used an established analytic framework[52,53] for time-frequency decomposition of motor-evoked activity to assess the spectral content of evoked activity. Using these methods, we were able to: (1) quantify the relationship between spiking and the LFP (that is, the SFC), (2) develop a model for how DCS effects neural circuits, and (3) link our findings with human ECoG recordings. All of this suggests that LFOs provide a useful framework for characterizing

important cortical dynamics during recovery. A final point in favor of this framework is that we found significant partial correlations between behavioral improvements separately for both the SFC and low-frequency LFP power; this suggests that specific aspects of the oscillatory dynamics (spiking and the LFP) provide independent explanatory power about motor recovery. This does raise a concern regarding the correct interpretation of the SFC. Specifically, task-evoked SFC could arise simply because both the LFP and spiking are phase locked to behavior, even if they are not directly related to each other. To address this, we subtracted the average ERP, which represents the phase-locked component of the LFP[53]; we still observed a task-related increase in power and the SFC, suggesting that the two signals are related to each other and not simply similarly phase locked to behavior. Together, our results indicate that the restoration of oscillatory dynamics observed both in spiking and in LFP data is important for motor recovery.

What is the possible relationship between LFOs, skilled behaviors and motor recovery? LFOs can be used to decode reach-related activity[7,14] and predict spiking phase across multiple behavioral states[7,14]. Such activity is also correlated with multiphasic muscle activations and movement timing[2,4,5,14,15]. Recent work also suggests that oscillatory dynamics reflect an underlying dynamical system[2]. This previous work argues that LFOs represent an intrinsic property of motor circuits associated with the precise temporal control of movements. Our findings extend this body of work by linking the restoration of LFO dynamics in the perilesional cortex to motor recovery. Our results directly implicate LFOs in the re-instantiation of cortical control of complex limb dynamics during reaching[17]. In our human stroke subject, persistent loss of cortical LFOs may suggest a mechanism for why reaching behaviors continued to be impaired. Of course, as we were only able to get data from one stroke patient, the generalizability of these findings remains unknown. The results need confirmation in a larger cohort. Nonetheless, given the concordance with our extensive rodent-based investigations, it is reasonable to propose that the recovery of LFOs may represent a marker of restored circuit dynamics after stroke, which is important for skilled reaching.

The exact origin of LFOs and the underlying generators remains unknown. Although our finding that a focal cortical stroke can perturb LFOs might indicate a local source, it is also increasingly clear that local perturbations can affect large-scale networks[19,54]. Indeed, reach-related LFOs may involve striatal[55] or thalamocortical activity[56], with impairments and recovery after stroke being functions of network plasticity rather than local effects restricted to M1. It is possible that these LFOs are related to slow cortical potentials associated with actions measured using EEG[22]. However, because those potentials may involve multiple cortical and/or subcortical networks, it is difficult to directly compare to our observed phenomenon. Further work specifically probing the interactions between the perilesional cortex and the broader motor network can clarify what drives our observed electrophysiological changes during recovery.

We found that pulses of DCS (for example, Fig. 6) could improve motor function when timed to start prior to and last through the reach period. How might electrical stimulation improve motor function after stroke, and how does this differ from previous neuromodulation methods in stroke[29,30,33,57]? In many previous animal and human studies (best exemplified in the EVEREST trial[30]), sub-threshold high-frequency epidural stimulation over the perilesional cortex was used to generally enhance cortical plasticity. Stimulation was delivered for an extended period of time in an 'open-loop' manner—that is, not timed with behavior—and the primary outcome measures were long-term changes in map plasticity (in animals[57]) and long-lasting changes in motor function (in both animals and humans)[30,57]. Such stimulation protocols are thought to induce lasting changes in excitability[31] that probably requires brain-derived neurotrophic factor[32]. A more novel form

of stimulation used a closed-loop paradigm in which stimulation in one region was linked with firing activity in a different region[33], but again, the primary goal was to induce long-term changes in network plasticity. In contrast to these previous efforts, our study was designed to test whether electrical stimulation could specifically modulate the brief, movement-locked neural activity identified here and thereby improve motor function—that is, apart from any long-term changes in cortical excitability or plasticity. Indeed, we show that brief, DCS pulses can modulate movement-locked, low-frequency activity and can improve motor function post-stroke. Thus, our study provides a theoretical basis for designing a rationale, on-demand and neutrally targeted stimulation paradigm for improving motor function. Moreover, our method of delivering stimulation (that is, via cranial screws) is potentially translatable as a novel class of invasive medical devices. Such a device could address growing concerns that non-invasive stimulation may not reliably modulate the cortex[58].

Stroke is one of the primary causes of long-term motor disability. Most current therapies, including task-specific rehabilitation training, are designed to enhance endogenous neural plasticity[59]. Here, we have identified a novel neurophysiological target and tested a dynamic neuromodulation approach for improving motor function post-stroke. Moreover, because LFOs can be recorded in human subjects both non-invasively (that is, task-evoked delta/theta power using EEG)[5] and invasively (that is, using ECoG)[8], there is a potential path to translate our results to stroke patients. These results may provide the basis for a new generation of 'smart' stimulation devices that can precisely target neuromodulation to improve motor function after stroke.

Methods

Methods, including statements of data availability and any associated accession codes and references, are available at https://doi.org/10.1038/s41591-018-0058-y.

References

1. Churchland, M. M., Cunningham, J. P., Kaufman, M. T., Ryu, S. I. & Shenoy, K. V. Cortical preparatory activity: representation of movement or first cog in a dynamical machine? *Neuron* **68**, 387–400 (2010).
2. Churchland, M. M. et al. Neural population dynamics during reaching. *Nature* **487**, 51–56 (2012).
3. Hall, T. M., de Carvalho, F. & Jackson, A. A common structure underlies low-frequency cortical dynamics in movement, sleep, and sedation. *Neuron* **83**, 1185–1199 (2014).
4. Bansal, A. K., Vargas-Irwin, C. E., Truccolo, W. & Donoghue, J. P. Relationships among low-frequency local field potentials, spiking activity, and three-dimensional reach and grasp kinematics in primary motor and ventral premotor cortices. *J. Neurophysiol.* **105**, 1603–1619 (2011).
5. Stefanics, G. et al. Phase entrainment of human delta oscillations can mediate the effects of expectation on reaction speed. *J. Neurosci.* **30**, 13578–13585 (2010).
6. Mollazadeh, M. et al. Spatiotemporal variation of multiple neurophysiological signals in the primary motor cortex during dexterous reach-to-grasp movements. *J. Neurosci.* **31**, 15531–15543 (2011).
7. Mollazadeh, M. et al. Coherency between spike and LFP activity in M1 during hand movements. in 2009 4th International IEEE/EMBS Conference on Neural Engineering, 506–509 (IEEE, 2009).
8. Ganguly, K. et al. Cortical representation of ipsilateral arm movements in monkey and man. *J. Neurosci.* **29**, 12948–12956 (2009).
9. Rickert, J. et al. Encoding of movement direction in different frequency ranges of motor cortical local field potentials. *J. Neurosci.* **25**, 8815–8824 (2005).
10. Donoghue, J. P., Sanes, J. N., Hatsopoulos, N. G. & Gaál, G. Neural discharge and local field potential oscillations in primate motor cortex during voluntary movements. *J. Neurophysiol.* **79**, 159–173 (1998).
11. O'Leary, J. G. & Hatsopoulos, N. G. Early visuomotor representations revealed from evoked local field potentials in motor and premotor cortical areas. *J. Neurophysiol.* **96**, 1492–1506 (2006).

12. Sasaki, K., Gemba, H. & Hashimoto, S. Premovement slow cortical potentials on self-paced hand movements and thalamocortical and corticocortical responses in the monkey. *Exp. Neurol.* **72**, 41–50 (1981).

13. Hashimoto, S., Gemba, H. & Sasaki, K. Analysis of slow cortical potentials preceding self-paced hand movements in the monkey. *Exp. Neurol.* **65**, 218–229 (1979).

14. Hall, T. M., Nazarpour, K. & Jackson, A. Real-time estimation and biofeedback of single-neuron firing rates using local field potentials. *Nat. Commun.* **5**, 5462 (2014).

15. Flint, R. D., Ethier, C., Oby, E. R., Miller, L. E. & Slutzky, M. W. Local field potentials allow accurate decoding of muscle activity. *J. Neurophysiol.* **108**, 18–24 (2012).

16. Krasoulis, A., Hall, T. M., Vijayakumar, S., Jackson, A. & Nazarpour, K. Generalizability of EMG decoding using local field potentials. in Engineering in Medicine and Biology Society (EMBC), 2014 36th Annual International Conference of the IEEE, 1630–1633 (IEEE, 2014).

17. Ramanathan, D., Conner, J. M. & Tuszynski, M. H. A form of motor cortical plasticity that correlates with recovery of function after brain injury. *Proc. Natl Acad. Sci. USA* **103**, 11370–11375 (2006).

18. Nudo, R. J., Wise, B. M., SiFuentes, F. & Milliken, G. W. Neural substrates for the effects of rehabilitative training on motor recovery after ischemic infarct. *Science* **272**, 1791–1794 (1996).

19. Lim, D. H., LeDue, J. M., Mohajerani, M. H. & Murphy, T. H. Optogenetic mapping after stroke reveals network-wide scaling of functional connections and heterogeneous recovery of the peri-infarct. *J. Neurosci.* **34**, 16455–16466 (2014).

20. Brown, C. E., Wong, C. & Murphy, T. H. Rapid morphologic plasticity of peri-infarct dendritic spines after focal ischemic. *Stroke* **39**, 1286–1291 (2008).

21. Rockstroh, B. *Slow Cortical Potentials and Behaviour* (Urban & Schwarzenberg, Munich, 1989).

22. Birbaumer, N., Elbert, T., Canavan, A. G. & Rockstroh, B. Slow potentials of the cerebral cortex and behavior. *Physiol. Rev.* **70**, 1–41 (1990).

23. *Preparatory States and Processes* (Psychology Press, Hillsdale, NJ, USA, 1984).

24. Honda, M. et al. Movement-related cortical potentials and regional cerebral blood flow change in patients with stroke after motor recovery. *J. Neurol. Sci.* **146**, 117–126 (1997).

25. Kitamura, J., Shibasaki, H. & Takeuchi, T. Cortical potentials preceding voluntary elbow movement in recovered hemiparesis. *Electroencephalogr. Clin. Neurophysiol.* **98**, 149–156 (1996).

26. Yilmaz, O., Birbaumer, N. & Ramos-Murguialday, A. Movement related slow cortical potentials in severely paralyzed chronic stroke patients. *Front. Hum. Neurosci.* **8**, 1033 (2015).

27. Yilmaz, O., Cho, W., Braun, C., Birbaumer, N. & Ramos-Murguialday, A. Movement related cortical potentials in severe chronic stroke. in Engineering in Medicine and Biology Society (EMBC), 2013 35th Annual International Conference of the IEEE, 2216–2219 (IEEE, 2013).

28. Allman, C. et al. Ipsilesional anodal tDCS enhances the functional benefits of rehabilitation in patients after stroke. *Sci. Transl Med.* **8**, 330re1 (2016).

29. Elsner, B., Kugler, J., Pohl, M. & Mehrholz, J. Transcranial direct current stimulation (tDCS) for improving activities of daily living, and physical and cognitive functioning, in people after stroke. *Cochrane Database Syst. Rev.* **3**, CD009645 (2016).

30. Levy, R. M. et al. Epidural electrical stimulation for stroke rehabilitation results of the prospective, multicenter, randomized, single-blinded Everest trial. *Neurorehabil. Neural Repair* **30**, 107–119 (2016).

31. Nitsche, M. A. & Paulus, W. Sustained excitability elevations induced by transcranial DC motor cortex stimulation in humans. *Neurology* **57**, 1899–1901 (2001).

32. Fritsch, B. et al. Direct current stimulation promotes BDNF-dependent synaptic plasticity: potential implications for motor learning. *Neuron* **66**, 198–204 (2010).

33. Guggenmos, D. J. et al. Restoration of function after brain damage using a neural prosthesis. *Proc. Natl Acad. Sci. USA* **110**, 21177–21182 (2013).

34. Reato, D., Rahman, A., Bikson, M. & Parra, L. C. Low-intensity electrical stimulation affects network dynamics by modulating population rate and spike timing. *J. Neurosci.* **30**, 15067–15079 (2010).

35. Ali, M. M., Sellers, K. K. & Fröhlich, F. Transcranial alternating current stimulation modulates large-scale cortical network activity by network resonance. *J. Neurosci.* **33**, 11262–11275 (2013).

36. Rosin, B. et al. Closed-loop deep brain stimulation is superior in ameliorating parkinsonism. *Neuron* **72**, 370–384 (2011).

37. Berényi, A., Belluscio, M., Mao, D. & Buzsáki, G. Closed-loop control of epilepsy by transcranial electrical stimulation. *Science* **337**, 735–737 (2012).

38. Whishaw, I. Q. & Pellis, S. M. The structure of skilled forelimb reaching in the rat: a proximally driven movement with a single distal rotatory component. *Behav. Brain Res.* **41**, 49–59 (1990).

39. Wong, C. C., Ramanathan, D. S., Gulati, T., Won, S. J. & Ganguly, K. An automated behavioral box to assess forelimb function in rats. *J. Neurosci. Methods* **246**, 30–37 (2015).

40. Kargo, W. J. & Nitz, D. A. Improvements in the signal-to-noise ratio of motor cortex cells distinguish early versus late phases of motor skill learning. *J. Neurosci.* **24**, 5560–5569 (2004).

41. Ramanathan, D. S., Gulati, T. & Ganguly, K. Sleep-dependent reactivation of ensembles in motor cortex promotes skill consolidation. *PLoS Biol.* **13**, e1002263 (2015).

42. Flint, R. D., Wright, Z. A., Scheid, M. R. & Slutzky, M. W. Long term, stable brain machine interface performance using local field potentials and multiunit spikes. *J. Neural Eng.* **10**, 056005 (2013).

43. Flint, R. D., Scheid, M. R., Wright, Z. A., Solla, S. A. & Slutzky, M. W. Long-term stability of motor cortical activity: implications for brain machine interfaces and optimal feedback control. *J. Neurosci.* **36**, 3623–3632 (2016).

44. Godlove, J., Gulati, T., Dichter, B., Chang, E. & Ganguly, K. Muscle synergies after stroke are correlated with perilesional high gamma. *Ann. Clin. Transl Neurol.* **3**, 956–961 (2016).

45. Gharbawie, O. A., Gonzalez, C. L. R., Williams, P. T., Kleim, J. A. & Whishaw, I. Q. Middle cerebral artery (MCA) stroke produces dysfunction in adjacent motor cortex as detected by intracortical microstimulation in rats. *Neuroscience* **130**, 601–610 (2005).

46. Carmichael, S. T. Rodent models of focal stroke: size, mechanism, and purpose. *NeuroRX* **2**, 396–409 (2005).

47. Nishibe, M., Edward, T. R., Urban, I., Barbay, S. & Nudo, R. J. Rehabilitative training promotes rapid motor recovery but delayed motor map reorganization in a rat cortical ischemic infarct model. *Neurorehabil. Neural Repair* **29**, 472–482 (2015).

48. Gulati, T. et al. Robust neuroprosthetic control from the stroke perilesional cortex. *J. Neurosci.* **35**, 8653–8661 (2015).

49. Chang, E. F. Towards large-scale, human-based, mesoscopic neurotechnologies. *Neuron* **86**, 68–78 (2015).

50. Bikson, M. et al. Effects of uniform extracellular DC electric fields on excitability in rat hippocampal slices in vitro. *J. Physiol.* **557**, 175–190 (2004).

51. Gulati, T., Ramanathan, D. S., Wong, C. C. & Ganguly, K. Reactivation of emergent task-related ensembles during slow-wave sleep after neuroprosthetic learning. *Nat. Neurosci.* **17**, 1107–1113 (2014).

52. Delorme, A. & Makeig, S. EEGLAB: an open source toolbox for analysis of single-trial EEG dynamics including independent component analysis. *J. Neurosci. Methods* **134**, 9–21 (2004).

53. Makeig, S. et al. Dynamic brain sources of visual evoked responses. *Science* **295**, 690–694 (2002).

54. Corbetta, M. et al. Common behavioral clusters and subcortical anatomy in stroke. *Neuron* **85**, 927–941 (2015).

55. DeCoteau, W. E. et al. Oscillations of local field potentials in the rat dorsal striatum during spontaneous and instructed behaviors. *J. Neurophysiol.* **97**, 3800–3805 (2007).

56. Dossi, R. C., Nuñez, A. & Steriade, M. Electrophysiology of a slow (0.5–4 Hz) intrinsic oscillation of cat thalamocortical neurones in vivo. *J. Physiol.* **447**, 215–234 (1992).

57. Plautz, E. J. et al. Effects of subdural monopolar cortical stimulation paired with rehabilitative training on behavioral and neurophysiological recovery after cortical ischemic stroke in adult squirrel monkeys. *Neurorehabil. Neural Repair* **30**, 159–172 (2016).

58. Lafon, B. et al. Low frequency transcranial electrical stimulation does not entrain sleep rhythms measured by human intracranial recordings. *Nat. Commun.* **8**, 1199 (2017).

59. Dimyan, M. A. & Cohen, L. G. Neuroplasticity in the context of motor rehabilitation after stroke. *Nat. Rev. Neurol.* **7**, 76–85 (2011).

Acknowledgements

Author contributions

For the rodent experiments, D.S.R., L.G., T.G., S.-J.W. and K.G. conceived and designed the experiments. R.A.S. provided input on the design of the stroke models. D.S.R., L.G., T.G., G.D., A.K.H. and S.-J.W. performed the experiments. D.S.R., L.G., G.D. and

Competing interests

Additional information

Supplementary information is available for this paper at https://doi.org/10.1038/s41591-018-0058-y.

Reprints and permissions information is available at www.nature.com/reprints.

Correspondence and requests for materials should be addressed to K.G.

Publisher's note: Springer Nature remains neutral with regard to jurisdictional claims in published maps and institutional affiliations.

Methods

Animal care and surgery. All procedures were in accordance with protocols approved by the Institutional Animal Care and Use Committee at the San Francisco Veterans Affairs Medical Center. Adult male Long Evans rats ($n = 34$, 250–400 g; Charles River Laboratories) were housed in a 12-h/12-h light–dark cycle. All surgical procedures were performed using a sterile technique under 2–4% isoflurane or a ketamine/xylazine cocktail. Surgery involved cleaning and exposure of the skull, preparation of the skull surface (using cyanoacrylate) and then implantation of the skull screws for referencing, stimulation and overall head-stage stability. Reference screws were implanted posterior to lambda and ipsilateral to the neural recordings. The ground screw was placed in the skull contralateral to the neural recordings and either placed posterior to lambda or over the nasal bone. For experiments involving physiological recordings, craniotomy and durectomy were performed, followed by implantation of the neural probes. The postoperative recovery regimen included the administration of 0.02 mg per kg body weight buprenorphine for 2 days, and 0.2 mg per kg body weight meloxicam, 0.5 mg per kg body weight dexamethasone and 15 mg per kg body weight trimethoprim sulfadiazine for 5 days. All animals were allowed to recover for 1 week prior to further behavioral training.

Behavior. Animals were acclimated and then trained to a plateau level of performance in a reach-to-grasp single-pellet task before neural probe implantation. Probe implantation was performed contralateral to the preferred hand. Animals were allowed to rest for 5 days before the start of experimental and/or recording sessions. During behavioral assessments, we monitored the animals and ensured that their body weights did not drop below 90% of their initial weight.

We used an automated reach-box, controlled by custom MATLAB scripts and an Arduino microcontroller. This setup required minimal user intervention, as described previously[39]. Each trial consisted of a pellet dispensed on the pellet tray, followed by an alerting beep indicating that the trial was beginning and then the door opening. Animals then had to reach their arm out, grasp and retrieve the pellet. A real-time 'pellet detector' using an infrared detector centered over the pellet was used to determine when the pellet was moved, which indicated that the trial was over and the door was closed. All trials were captured by video, which was synced with the electrophysiology data using Arduino digital output. The video frame rate was 30 Hz for the animals in the photothrombotic stroke electrophysiology experiments ($n = 6$), and 75 Hz for those in the MCA stroke electrophysiology experiments ($n = 4$) and stimulation experiments ($n = 14$). Physiological data presented in this paper were generally time locked to the onset of the reach movement. The onset of reach was determined manually from a recorded video and defined as the start of paw advancement towards the slot.

In vivo electrophysiology. We recorded extracellular neural activity using tungsten microwire electrode arrays (Tucker-Davis Technologies). We used either 16- or 32-channel arrays (33-μm polyamide-coated tungsten microwire arrays). Arrays were lowered down to a depth of ~1,200–1,500 μm. In healthy animals, neural probes were centered over the forelimb area of M1 (ref.[17]), at 3 mm lateral and 0.5 mm anterior from the bregma. In photothrombotic stroke animals, the neural probe was placed immediately anterior to the stroke site, typically centered ~3–4 mm anterior and 2.5–3 mm lateral to the bregma.

Units and LFP activity were recorded using a 128-channel TDT-RZ2 system (Tucker-Davis Technologies). Spike data were sampled at 24,414 Hz and LFP data at 1,017.3 Hz. ZIF clip-based analog head stages with a unity gain and high impedance (~1 GΩ) were used. The threshold for spiking activity was set online using a standard deviation of 4.5 (calculated over a 1-min period using the TDT-RZ2 system), and waveforms and timestamps were stored for any event that crossed that threshold. Sorting was performed using Plexon OfflineSorter v4.3.0, using a principal component analysis (PCA)-based method followed by manual inspection and sorting. We included both clearly identified single-units and multi-unit activity for this analysis (results were pooled as there were no clear differences in single-unit and multi-unit responses). A total of 171 single units and multi-units were recorded from healthy animals, 53 from those same animals post-MCA stroke, 170–219 from animals after photothrombotic stroke and 50 units in the ketamine experiment (only single units with a signal-to-noise ratio of >5.5 were used in this DCS experiment to minimize stimulated-related contamination of neural signals). Behavior-related timestamps (that is, trial onset and trial completion) were sent to the RZ2 analog input channel using an Arduino digital board and synchronized to neural data.

MCA stroke. For this procedure[60], adult rats were placed in the supine position and a ventral cervical midline skin incision was made under the surgical microscope. Both of the common carotid arteries were carefully isolated from the adjacent vagus nerve. The animal was then placed in the lateral position and an incision was made over the temporalis muscle, which was then retracted. The main trunk of the left MCA was exposed and occluded with an AVM micro clip (Codman & Shurtleff) and the common carotid arteries were occluded using micro clamps, both for 60 min. After ischemia, the micro clip and micro clamps were removed to restore blood flow after which the wound was sutured. This procedure has been previously shown to result in long-term loss of cortical tissue and long-term impairments in motor cortical function[61].

Photothrombotic stroke and electrophysiology. After craniotomy, rose bengal dye was injected into the femoral vein using an intravenous catheter. Next, the surface of the brain was illuminated with white light (KL-1500 LCD, Schott) using a fiber optic cable for 20 min. We used a 4-mm aperture for stroke induction (centered in the M1 area based on stereotactic coordinates) and covered the remaining cortical area with a custom aluminum foil mask to prevent light penetration. After induction, a probe was implanted in the perilesional cortex immediately anterior to the stroke site[48]. The craniotomy or implanted electrodes were covered with a layer of silicone (Quiksil), followed by dental cement.

DCS. _Anesthesia (ketamine) experiment._ Animals ($n = 10$) were initially anesthetized using a ketamine–xylazine cocktail (85 mg per kg ketamine and 10 mg per kg xylazine), with supplementary ketamine given every ~40–60 min as needed to maintain a stable anesthetic level and also to maintain anesthesia at stage III, which is characterized by predominantly slow oscillations[62]; 0.05 mg per kg atropine was also given separately to help to decrease secretions and counteract cardiac and respiratory depression. After anesthesia and craniotomy was performed, epidural stimulation electrodes were implanted (using cranial screws embedded in the skull) in the configuration noted in Fig. 5. The ground screw for this and all other stimulation experiments was implanted over the contralateral nasal bone, suggesting that current flow would probably go through the cortex and associated pathways in an anterior–medial direction from the site of stimulation. These screws were connected to a Multi-Channel Systems Stimulus Generator (MCS STG4000 series) to deliver DCS. In 3 animals, a ~2-mm tungsten wire was placed on the epidural surface in the craniotomy well instead of using skull screws to deliver the electrical stimulation. 32-channel multi-electrode arrays were implanted into layer V of the motor cortex (1,200–1,500-μm deep). Single-unit and LFP activities were recorded for 1 h to ensure the stability of recordings and to minimize drift during the stimulation experiment. Then, we recorded a baseline period of neural activity (~15 min), followed by neural activity during DCS (typically using 10–100-μA currents, applied for 1–5 min).

In vivo DCS experiments. Fixed-stimulation behavioral experiments. After a stroke was induced (photothrombotic: $n = 4$ and distal MCA: $n = 3$), two stainless steel skull screws were implanted 1 mm anterior and posterior to the stroke site; we ensured that the electrodes were as close as possible to the stroke site and that they were located near the midline of the stroke area. The ground screw was implanted over the contralesional nasal bone. Following a 1-week recovery period, animals were tested several times each week, and those showing no persistent motor deficit ($n = 3$) were excluded from further testing. Animals were tested until their behavior was at a plateau, with reach accuracies at least >15%. DCS, applied using an IZ2 stimulus isolator (Tucker-Davis Technologies), was administered on both variable and fixed schedules. Stimulation was delivered on two screws in each animal, with a maximum stimulation amplitude of 200 μA per screw. Pilot studies in the first two animals suggested that accuracy on the skilled forelimb reach task was improved with >150 μA of current per screw; based on this pilot data, we provided at least 150 μA of current per screw in all animals undergoing behavioral testing. The stimulation current was increased up to the point of tolerability by the subject, with a maximum amplitude of 200 μA per screw. Tolerability was defined as animals not making any observable behavioral response to the onset or offset of the stimulation pulse. We tested both cathodal and anodal polarities of stimulation, as described in the Results section and below.

The current densities used in our study seem to be less that what has been used in previous studies. For example, a 2016 study used epidural electrodes for language mapping[63]. The authors report using 5–15 mA of current delivered through 2.3-mm electrodes (an area of 4.15 mm²); this results in a current density of 2.4 mA per mm². Similarly, the current densities used for epidural stimulation in the Everest trial were also comparable[30]. The study reported using currents up to 13 mA using four electrodes with a 3-mm diameter. Thus, each electrode could have a density of 0.46 mA per mm². There are also multiple non-human primate studies using epidural stimulation. We estimate the following densities for the two example studies: 0.92 mA per mm² (ref.[64]) and 1.41 mA per mm² (ref.[65]). In comparison, we used 1-mm diameter screws. We typically used between 150 and 200 μA per skull screw when delivering stimulation. Our estimated current density was 0.25 mA per mm². Thus, to the best of our knowledge, our current densities are comparable to those used in invasive human and non-human primate studies. Fixed stimulation ($n = 7$; data in Fig. 6a–c) began 500 ms prior to the door opening (that is, the signal for the trial starting) and lasted up to 5 s total (encompassing the entire reach period, with stimulation turned off after the trial ended). Thirty trial blocks of stimulation 'on', 'off' and 'sham' (a 200-ms pulse that ended prior to the door opening, to mimic the sensory or possible alerting effects of the stimulation onset) were counterbalanced and interleaved across days. The effects of stimulation and sham were made based on the per cent improvements compared to temporally adjacent no stimulation blocks. We made a decision to randomize at the level of blocks (that is, blocks of 30 trials for fixed stimulation experiments; 25 trials in DCS with the physiology experiments) rather than at the level of trials because of the pilot data (in 2 animals), which had more robust behavioral effects when randomized in this manner.

Because we performed stimulation or sham stimulation sessions across days, we also calculated the standard deviation in the percentage improvement for each animal across days to see whether this differed between conditions. We did not find a significant difference between the two conditions ($t(6) = 1.37$, $P = 0.21$). We did observe improvements in performance in both stroke models, with no significant differences by stroke model type ($t(5) = 1.24$, $P = 0.271$). Although the above experiments were all conducted using cathodal stimulation, we found similar effects using the anodal stimulation condition (anodal stimulation showed an improvement of $60 \pm 12\%$ (one-sample t-test: $t(4) = 4.95$, $P = 0.008$; $n = 5$ animals, which included experiments performed in two of the animals used above for cathodal stimulation and 3 additional animals, all in a photothrombotic stroke model). There was no difference between anodal and cathodal stimulation on motor improvement (analysis of variance (ANOVA), $t(10) = 0.736$, $P = 0.479$).

Joint stimulation physiology experiments. In studies combining electrophysiology and DCS ($n = 4$; Fig. 6d,e), we found that high-stimulation currents resulted in artifacts that were difficult to remove. For this reason, we utilized smaller currents ($81.654 \pm 12.414 \mu A$ mean current amplitudes in these experiments versus $321.4 \pm 12.2 \mu A$ in the behavioral experiments above), with the primary goal of understanding whether DCS could affect the LFO in any way. DCS started 9 s before the door opened for the reach to start and lasted 7 s after the door opened in these experiments, to minimize stimulation-related artifacts in LFP recordings of interest ($n = 4$ rats, data in Fig. 6d,e). Photothrombotic stroke was used in the joint stimulation and physiological recording experiments ($n = 4$). Furthermore, as the aim was to see whether the LFO was boosted with DCS, in these experiments, we started testing immediately after stroke (after a 14-day recovery period). For all fixed-stimulation DCS experiments, the stimulation screws were placed anterior or posterior to the lesion or the electrodes, and the 'ground screw' was placed on the contralateral hemisphere on the nasal bone. For the joint stimulation and physiology experiments, the stimulation screws were placed somewhat diagonally and at a further distance from the stroke to accommodate recording array. Thus, the fixed stimulation versus joint stimulation and recording were optimized for behavioral effects versus physiological recordings or effects, respectively.

Variable stimulation experiment. Variable timing stimulation ($n = 4$; Fig. 6f,g) began at 6 time points with respect to door open (-1s, -0.5s, 0 s, 0.5 s, 1 s and 1.5 s) and lasted 1 s to ensure a spread of temporal relationships between stimulation start and reach onset (ΔT). Stimulation was delivered in blocks of 25 trials with stimulation start time consistent within-block. Animals underwent 12 random-ordered blocks each day with each time point tested in a total of 50 trials in 2 non-consecutive blocks. For each trial in each animal, we calculated the exact ΔT for analysis. Data were pooled in each animal from both the anodal and the cathodal stimulation experiments; there was no evidence that one form of stimulation worked consistently or significantly more than the other, which is consistent with data from the longer-duration stimulation experiments described above. Because there is some variability between the trial start (that is, door opening) and the actual reach onset, the exact ΔT varied quite a bit from trial to trial even in the same stimulation block, thus helping to increase the randomization of this experiment.

Immunohistochemistry. Rats were anesthetized and transcardially perfused with 0.9% sodium chloride, followed by 4% formaldehyde. The harvested brains were post-fixed for 24 h and immersed in 20% sucrose for 2 days. Coronal cryostat sections (40-μm thickness) were incubated with blocking buffer (10% Donkey serum and 0.1% Triton X-100 in 0.1 M phosphate buffer) for 1 h and then incubated overnight with mouse anti-NeuN (1:1,000; Millipore). After washing, the sections were incubated with biotinylated anti-mouse IgG secondary antibody (1:300; Vector Lab) for 2 h. Sections were incubated with avidin–biotin peroxidase complex reagents using a Vector ABC kit (Vector Labs). The horseradish peroxidase reaction was detected with diaminobenzidine and H_2O_2. The sections were washed in phosphate buffer and then mounted with permount solution (Fisher Scientific) on superfrosted coated slides (Fisher Scientific). The images of a whole section were taken by a HP scanner, and the microscope image was taken by a Zeiss microscope.

Human ECoG experiments. We utilized data that had been collected and described in two previous papers[8,44]. As previously described, these studies were conducted using a protocol approved by the UCSF CHR (Committee on Human Research); all subjects were conducted after obtaining informed consent from subjects. Data were collected from two subjects without stroke and one subject with documented cortical stroke. All subjects had epilepsy and had chronic ECoG grids implanted for pre-surgical monitoring or localization of the seizure. Consent and details of recordings and of the specific aspects of the behavioral paradigm in healthy subjects were previously reported[8], as well as previously reported for the stroke subject[44]. In brief, all subjects performed a center-out reaching task, in which trials began with the appearance of a target at the center of the reach field, followed, after a variable delay, with a cue indicating that the subjects should perform a reach to one of four targets.

Data analysis. *LFP/ECoG and single-unit analyses.* Analyses were conducted using a combination of custom-written routines in MATLAB 2015a/2017a (Math Works), along with functions or routines from the EEGLAB toolbox (http://sccn.ucsd.edu/eeglab/) and the Chronux toolbox (http://chronux.org/). Pre-processing steps for LFP/ECoG analysis included: artifact rejection (removing broken channels and noisy trials); Z scoring; and common-mode referencing using the median signal (at every time point, the median signal across the remaining electrodes was calculated, and this median signal was subtracted from every channel to decrease the common noise and minimize volume conduction). We used median referencing rather than mean referencing to minimize the effect of channels with high noise or impedance that were not discarded). For the joint stimulation and physiology experiments, we witnessed crosstalk between channels in two animals, and thus non-median subtracted LFP was analyzed. Filtering of data at specified frequency bands was performed using the EEGLAB function eegfilt(). Calculation of power was performed with wavelets using the EEGLAB function newtimef(). All time–frequency decompositions were performed on data on a trial-by-trial basis to capture the 'total power' (that is, both phase locked ('evoked') and non-phase locked ('induced')) power. To isolate and also study only the 'induced' oscillatory activity, we performed a similar analysis after subtracting the mean evoked potential from the single-trial data. By subtracting this out, we removed, for each trial, the predominant phase-locked activity in the LFP, and what remained was the 'induced' activity in which power increased in a non-phase-locked manner. Channels used for ECoG analysis were chosen by locating, for each subject, the central sulcus and selecting anatomically adjacent electrodes both anterior and posterior to the central sulcus. We performed the analysis using electrodes as far ventral as the Sylvian fissure for this paper; however, we also performed an analysis in which we subsampled only the dorsal half of these electrodes from each subject, presumably closer to the hand knob, and found similar results.

Statistical quantification of how stroke and recovery affected power and the SFC in rodents was calculated by taking the mean power or the SFC from -0.25 s to 0.75 s around the reach onset. Only trials where the rat managed to at least touch and knocked off the pellet were included in the analysis. In Fig. 1, the baseline period is -3 s to -2 s relative to the reach onset. In Fig. 2, quantifications were made between all valid trials (at least 50) in the recording block before and after the stroke. In Fig. 3, comparisons were made across the first 50 and the last 50 trials or the first and last recording block, for power and the SFC, respectively, for each animal. In humans, we used data from -0.3 s to 0.3 s from the reach onset across all trials performed in each subject. Calculation of SFC values was performed using the Chronux function cohgramcpt. For awake task-related experiments, SFC calculations were performed using 1-s windows moving by 0.025 s. For the anesthetized DCS experiments, multitaper and window parameters used for sleep-epoch analyses were utilized[51,66].

Sorted spikes were binned at 20 ms unless otherwise stated. After spikes were time locked to behavioral markers, the peri-event time histogram was estimated by Bayesian adaptive regression splines[67]. Unit modulation was calculated as (maximum − minimum)/(maximum + minimum) firing rate from -4 s to 2.5 s around reach, after spline fitting. Gaussian process factor analysis[68], in Supplementary Fig. 1, was done using DataHigh[69], with spikes from -1 s to 1.5 s around grasp onset.

Spike-phase histograms in Supplementary Figs. 3 and 4 were calculated by first taking the Hilbert transform of the LFP filtered from 1.5–4 Hz and then finding the phases of the LFP at which spikes (between -0.25 s and 0.75 s from the reach onset) occurred. For every spike–LFP pair (all spikes and LFP channels from each animal, across all four animals), we calculated the Rayleigh's Z statistic for circular non-uniformity and then obtained the percentage of significant pairs ($P < 0.05$).

Statistical analysis. Parametric statistics were generally used in this study (ANOVA, t-tests, Pearson's correlation and linear regression, unless otherwise stated), implemented within either MATLAB or SPSS. The linear mixed-effects model (implemented using MATLAB fitlme) was used to compare the differences in unit modulation, SFC and LFP power in Figs. 1–3 and the LFP power for stimulation on and off trials in Fig. 6. This model accounts for the fact that units, channels or trials from the same animal are more correlated than those from different animals and is more stringent than computing statistical significance over all units, channels and trials[70]. We fitted random intercepts for each rat and reported the P values for the regression coefficients associated with pre-stroke or post-stroke, early or late recovery, or stimulation on or off.

In Fig. 4, we used anatomically defined sensorimotor electrodes (electrodes that laid on either side of the central sulcus) and performed an ANOVA between conditions (stroke versus non-stroke), with subject included as an additional factor. In Fig. 5, we analyzed data from only one channel in each animal (non-referenced) and calculated parametric statistics across animals (Fig. 5b) or units (Fig. 5d). In Fig. 6, we performed parametric statistics across animals. In Fig. 6f,g, to calculate significance, we performed two-tailed, one-sample t-tests at each time point displayed followed by Bonferroni–Holm correction for family-wise error. To confirm the effect, using a permutation test, we performed the following analysis. For each trial in each animal, we calculated the ΔT and the accuracy (success or fail) of that trial. We then randomized the accuracies relative to the ΔT 1,000 times for each animal, maintaining in each animal the overall distribution of times (that is,

ΔT and accuracy). Then, we computed for each animal the percentage accuracy at any particular ΔT (around a window of ± 50 ms) and also the 1,000 surrogate (that is, randomized) accuracy at these time points. Across animals, we then calculated the mean accuracy and compared this to the distribution of mean accuracies across the four animals generated from the randomized surrogates. Significance was assigned according to two-tailed probabilities, such that at any point in time, accuracy more than or less than the 97.5th percentile in either direction at that particular ΔT was assigned a significance of <0.05. The significance values derived from this approach are more conservative than the P values derived from a more standard one-sample t-test at each time point, and likewise confirmed significance of the time point in question (-450 ms prior to the reach onset).

Reporting Summary. Further information on experimental design is available in the Nature Research Reporting Summary linked to this article.

Data availability. The data sets generated during (i.e., all the rodent data shown in this paper) and/or analyzed (i.e., human ECoG data) during the current study (and the associated custom code created in MATLAB) are available from the corresponding author on reasonable request.

References

60. Longa, E. Z., Weinstein, P. R., Carlson, S. & Cummins, R. Reversible middle cerebral artery occlusion without craniectomy in rats. *Stroke* **20**, 84–91 (1989).
61. Rogers, D. C., Campbell, C. A., Stretton, J. L. & Mackay, K. B. Correlation between motor impairment and infarct volume after permanent and transient middle cerebral artery occlusion in the rat. *Stroke* **28**, 2060–2066 (1997).
62. Friedberg, M. H., Lee, S. M. & Ebner, F. F. Modulation of receptive field properties of thalamic somatosensory neurons by the depth of anesthesia. *J. Neurophysiol.* **81**, 2243–2252 (1999).
63. Taplin, A. M. et al. Intraoperative mapping of expressive language cortex using passive real-time electrocorticography. *Epilepsy Behav. Case Rep.* **5**, 46–51 (2016).
64. Plautz, E. J. et al. Post-infarct cortical plasticity and behavioral recovery using concurrent cortical stimulation and rehabilitative training: a feasibility study in primates. *Neurol. Res.* **25**, 801–810 (2003).
65. Levy, R. et al. Cortical stimulation for the rehabilitation of patients with hemiparetic stroke: a multicenter feasibility study of safety and efficacy. *J. Neurosurg.* **108**, 707–714 (2008).
66. Gulati, T., Guo, L., Ramanathan, D. S., Bodepudi, A. & Ganguly, K. Neural reactivations during sleep determine network credit assignment. *Nat. Neurosci.* **20**, 1277–1284 (2017).
67. Wallstrom, G., Liebner, J. & Kass, R. E. An implementation of Bayesian adaptive regression splines (BARS) in C with S and R wrappers. *J. Stat. Softw.* **26**, 1–21 (2008).
68. Yu, B. M. et al. in *Advances in Neural Information Processing Systems 21* (eds. Koller, D. et al.) 1881–1888 (Curran Associates, Inc., Red Hook, NY, USA, 2009).
69. Cowley, B. R. et al. DataHigh: graphical user interface for visualizing and interacting with high-dimensional neural activity. *J. Neural Eng.* **10**, 066012 (2013).
70. Aarts, E., Verhage, M., Veenvliet, J. V., Dolan, C. V. & van der Sluis, S. A solution to dependency: using multilevel analysis to accommodate nested data. *Nat. Neurosci.* **17**, 491–496 (2014).

nature research

Corresponding author(s): Karunesh Ganguly

Reporting Summary

Nature Research wishes to improve the reproducibility of the work that we publish. This form provides structure for consistency and transparency in reporting. For further information on Nature Research policies, see Authors & Referees and the Editorial Policy Checklist.

Statistical parameters

When statistical analyses are reported, confirm that the following items are present in the relevant location (e.g. figure legend, table legend, main text, or Methods section).

n/a	Confirmed
☐	☒ The exact sample size (n) for each experimental group/condition, given as a discrete number and unit of measurement
☐	☒ An indication of whether measurements were taken from distinct samples or whether the same sample was measured repeatedly
☐	☒ The statistical test(s) used AND whether they are one- or two-sided *Only common tests should be described solely by name; describe more complex techniques in the Methods section.*
☐	☒ A description of all covariates tested
☐	☒ A description of any assumptions or corrections, such as tests of normality and adjustment for multiple comparisons
☐	☒ A full description of the statistics including central tendency (e.g. means) or other basic estimates (e.g. regression coefficient) AND variation (e.g. standard deviation) or associated estimates of uncertainty (e.g. confidence intervals)
☐	☒ For null hypothesis testing, the test statistic (e.g. F, t, r) with confidence intervals, effect sizes, degrees of freedom and P value noted *Give P values as exact values whenever suitable.*
☐	☒ For Bayesian analysis, information on the choice of priors and Markov chain Monte Carlo settings
☐	☒ For hierarchical and complex designs, identification of the appropriate level for tests and full reporting of outcomes
☐	☒ Estimates of effect sizes (e.g. Cohen's d, Pearson's r), indicating how they were calculated
☐	☒ Clearly defined error bars *State explicitly what error bars represent (e.g. SD, SE, CI)*

Our web collection on statistics for biologists may be useful.

Software and code

Policy information about availability of computer code

Data collection	We use MATLAB 2014a to run the automated rodent reaching box (Wong et al., 2015). We use TDT OpenEx Software Suite to collect neurophysiology data.
Data analysis	We used MATLAB 2015b and 2017a for data analyses in this manuscript. This includes both standard toolboxes others have developed (particularly EEGLab, https://sccn.ucsd.edu/eeglab/) and Chronux (http://chronux.org/). Custom scripts were developed for analyses specific to the animals/behavioral paradigms analyzed here, and will be made available on request. We used SPSS 20 for some statistical analyses. We also used DataHigh v1.2 for Gaussian Process Factor Analysis in Supp Fig. 1.

For manuscripts utilizing custom algorithms or software that are central to the research but not yet described in published literature, software must be made available to editors/reviewers upon request. We strongly encourage code deposition in a community repository (e.g. GitHub). See the Nature Research guidelines for submitting code & software for further information.

Data

Policy information about availability of data

All manuscripts must include a data availability statement. This statement should provide the following information, where applicable:

- Accession codes, unique identifiers, or web links for publicly available datasets
- A list of figures that have associated raw data
- A description of any restrictions on data availability

> The datasets generated during and/or analysed during the current study are available from the corresponding author on reasonable request.

Field-specific reporting

Please select the best fit for your research. If you are not sure, read the appropriate sections before making your selection.

☒ Life sciences   ☐ Behavioural & social sciences

For a reference copy of the document with all sections, see nature.com/authors/policies/ReportingSummary-flat.pdf

Life sciences

Study design

All studies must disclose on these points even when the disclosure is negative.

Sample size	Sample sizes were chosen based on previous experiments we conducted in stroke animals (Gulati et. al., J. Neurosci, 2014). In that paper, the physiological (single units, LFP power/phase) changes observed after stroke were significantly large that 4 animals/group were sufficient to perform the relevant analyses. Thus, for all major claims about rodents, we ensured there were at least 4 animals/group (for some experiments, we conducted experiments in greater than 4 animals). For human studies, we conducted analyses "within-subect", across electrodes. Because these studies were conducted using ECoG neural probes in patients with a seizure focus over sensorimotor cortex, we were inherently limited in the number of subjects we could recruit.
Data exclusions	In Figs 1 - 2, 4 - 6 no data was excluded. In Fig 3, 7 animals were excluded as they did not experience any motor deficits after the procedure. In a subset we verified that indeed no stroke had occurred. We thus included only animals with clear deficits after the procedure (n=6). In Fig 7, one animal (out of 5) had several sessions excluded due to the stimulation experiment not working appropriately (lower current than desired was being passed due to problems with electrode impedance, but this was only realized after data collection had been finished for that animal, so we could not perform more experimental sessions).
Replication	We have presented all of the data we collected in the paper. There were no other attempts to reproduce the data.
Randomization	Randomization/blinding is most relevant from the perspective of the treatment studies (i.e., electrical stimulation). During treatments involving electrical stimulation, randomization occurred within the animal (on some trials animals received stimulation and other trials it did not, and we compared performance between those conditions). These experimental sessions were "pseudo-randomized", in that, across blocks of 30 trials, a different experimental condition was used, and the order of conditions was different across different days for the same animal.
Blinding	For stimulation studies, we have several markers indicating when the pulse is coming on/off (in order to ensure appropriate delivery), so investigator was not blinded to which trials stimulation was occurring. However, the behavioral task is fully automatic once started and does not require experimenter intervention. The metric of accuracy (whether the animal retrieved the pellet or not) is also quite objective. Moreover, data was collected by 3 different people across different animals, and similar effects of stimulation were observed.

Materials & experimental systems

Policy information about availability of materials

n/a	Involved in the study
☒	☐ Unique materials
☐	☒ Antibodies
☒	☐ Eukaryotic cell lines
☐	☒ Research animals
☐	☒ Human research participants

Antibodies

Antibodies used	Mouse anti-NeuN, Millipore, MAB377, clone A60, dilution 1:1000 Biotinylated anti-mouse IgG, Vector Labs, BA-2000, lot no. ZA0409, dilution 1:300
Validation	Anti-NeuN Antibody, clone A60 detects level of NeuN and has been published and validated for use in FC, IC, IF, IH, IH(P), IP and

WB. More information and references can be found on manufacturer's website (http://www.emdmillipore.com/US/en/product/Anti-NeuN-Antibody-clone-A60,MM_NF-MAB377).

Research animals

Policy information about studies involving animals; ARRIVE guidelines recommended for reporting animal research

Animals/animal-derived materials	In this experiment, we used male Long-Evans rats. There were housed in a 12h:12h light/dark cycle room. Animals were purchased as 3-4 months old adults between 250 - 300 grams.

Human research participants

Policy information about studies involving human research participants

Population characteristics	We had three human research participants, all with epilepsy, who volunteered to be research subjects while undergoing a week long ElectroCorticography implantation over sensorimotor cortex in an attempt to localize the seizure foci. The subjects were all male. One subject had a stroke over M1; the other two had no observable lesion within M1 or any other motor structure, and were used as intact controls.

Method-specific reporting

n/a	Involved in the study
☒	☐ ChIP-seq
☒	☐ Flow cytometry
☒	☐ Magnetic resonance imaging